Asian Journal of Chemistry; Vol. 33, No. 10 (2021), 2365-2372

ASIAN JOURNAL OF CHEMISTRY

https://doi.org/10.14233/ajchem.2021.23334

Electronic Transitions, Inter- and Intra-Bond Interactions of an Azabicycle Single Crystal using DFT

J. DINESHKUMAR[1], S. SUBASHCHANDRABOSE[2], S. NIAZ[3] and P. PARTHIBAN[1,*]

[1]Department of Chemistry, Centre for R&D, PRIST (Deemed University), Thanjavur-613403, India
[2]Department of Physics, Centre for R&D, PRIST (Deemed University), Thanjavur-613403, India
[3]Department of Physics, University of Sargodha, Sub-campus Bhakkar, 30000, Pakistan

*Corresponding author: E-mail: parthisivam@yahoo.co.in

Received: 24 May 2021; *Accepted*: 20 July 2021; *Published online*: 20 September 2021; AJC-20508

2,4-Diphenyl-3-azabicyclo[3.3.1]nonan-9-one O-benzyloxime (ABN-OBn) was synthesized by modified Mannich condensation, purified by recrystallization and single crystals were grown by slow evaporation from ethanol. The empirical formula of the molecule is $C_{27}H_{28}N_2O$ as witnessed by HRMS, elemental analysis and the X-ray diffraction. The crystal belongs to triclinic system ($\alpha = 73.640$, $\beta = 78.505$, $\gamma = 87.078$) with P-1 space group. The electronic excited states of ABN-OBn have been calculated using TD-DFT/B3LYP/6-31G(d,p) level of theory, in order to investigate the electronic transitions within the molecule. Frontier molecular orbitals (FMOs) of ABN-OBn have been studied to understand the electronic charge distributions and its band gap (5.0514 eV/245.45 nm). Density of states (DOS), partial density of states (PDOS) and total density of states (TDOS) with respect to functional groups were computed to investigate the electron densities of functional groups in the molecule. Natural bond orbital (NBO) has been performed to explore the intramolecular π-π* interaction of the compound.

Keywords: Azabicycle, Crystal structure, Hirshfeld surface analysis, Computational study, DFT.

INTRODUCTION

Azabicyclononanes (ABNs) are present in the naturally occurring alkaloids, having a broad spectrum of medicinal activities such as antibacterial, antifungal, antituberculostic, analgesic, antioxidant, antitussive, anti-inflammatory, antipyretic, antiphologistic, sedatives, calcium antagonist, hypotensive, narcotic antagonism and local anesthetic, *etc.* [1-7].

By considering the importance, synthesis of ABNs is a parallel practice to the more complex isolation of ABN molecules in nature [8-11]. By optimized the modified Mannich reactions, we already reported a range of functionalized/highly functionalized ABNs [12-14]. In this article, we discussed the theoretical studies of the conveniently synthesized/biologically potent ABN-OBn molecule (oxime ether derivative of ABN); it contains functionalized ABN moiety and an active oxime ether pharmacophore of the Oxiconazole, an antifungal drug. It is a fact that the biological actions of any molecule mainly depend on the stereochemistry of molecule and very significantly, the physico-chemical parameters are very vital in drug design, analysis and delivery [15-17].

Due to our interest in NMR spectral studies of oxime ethers of various nitrogen heterocycles [12-15,18-21], we synthesized and reported the complete ^1H & ^{13}C NMR spectral studies of a series of 2,6-diarylpiperidin-4-one O-benzyloximes, 2,4-diaryl-3-azabicyclo[3.3.1]nonan-9-one O-benzyloximes and 2,4,6,8-tetraaryl-3,7-diazabicyclo[3.3.1]nonan-9-one O-benzyloximes [12]. 2,4-Diphenyl-3-azabicyclo[3.3.1]nonan-9-one O-benzyl oxime (ABN-OBn) is studied by computational analysis and compared with the crystallographic data. To our best, it is the first computational study for this class of bicyclic molecules of biological importance.

Further, we explored certain physico-chemical parameters (not only for the biological perspectives, even for material science applications) such as geometry of the molecule, structural property due to various functional groups, band gap, electronic excitations (in singlet and triplet) and their energy

transitions, non-linear optical activity using hyper-polar coefficient and electron density analysis.

EXPERIMENTAL

Synthesis of 2,4-diphenyl-3-azabicyclo[3.3.1]nonan-9-one (ABN): Mixture of cyclohexanone, benzaldehyde and ammonium acetate in 1:2:1.5 ratios in ethanol were gently warmed and stirred until the completion of the reaction. Thus, the formed crude product was filtered and washed with ethanol, ether (1:5) mixture [15]. The bicyclic ketone then recrystallized from ethanol to obtain pure compound.

Synthesis of 2,4-diphenyl-3-azabicyclo[3.3.1]nonan-9-one O-benzyloxime (ABN-OBn): A mixture of 2,4-diphenyl-3-azabicyclo[3.3.1]nonan-9-one (5 mmol), O-benzyl hydroxylamine hydrochloride (5 mmol) and sodium acetate trihydrate (15 mmol) in methanol was refluxed till completion of the reaction. After that water added to the reaction mixture and extracted with ether, dried with anhydrous sodium sulphate and evaporated. Thus, the obtained crude oxime ether ABN-OBn was recrystallized from ethanol and slowly evaporated to obtain the diffraction quality crystals [15].

Computational details: The quantum chemical calculations of ABN-OBn were performed using the B3LYP level of theory supplemented with 6-31G(d,p) basis set, using Gaussian 03 program package invoking geometry optimization [22]. Initial geometry generated from geometrical parameters was minimized without any constraint in the potential energy surface at DFT level. Hirshfeld surface maps and fingerprint plots were generated from the crystallographic data using the Crystal Explorer 3.1 [23].

RESULTS AND DISCUSSION

Molecular geometry: The ABN-OBn crystal structure belongs to a triclinic system ($\alpha = 73.640$, $\beta = 78.505$, $\gamma = 87.078$) with P-1 space group. The lattice cell parameters are a = 8.6884 (7), b = 9.6961, c = 14.1567 (Å) and the symmetry code of the molecule in the crystal unit is (i) x-1/2, -y+1/2, z+3/2; (ii) x+1/2, -y+1/2, z-1/2; (iii) x+1, y, z-1; (v) x-1, y, z+1. Crystallographic parameters are provided in Table-1. The conformation of piperidine and cyclohexane rings of the ABN-OBn was analyzed with the puckering parameters (Table-2a), proposed by Cremer & Pople [24]. Accordingly, conformation of the substituted piperidone ring (C1–C2–C3–C4–C5–N1) was found to be a chair with the total puckering amplitude Q_T = 0.575(9) Å and the phase angle θ = 3.9(9)º, φ = 190º(14); fairly deviated from the ideal chair of cyclohxane (for the ideal chair, Q_T = 0.630 Å and θ = 0º or 180º) [24].

The conformation of cyclohexane (C2–C3–C4–C6–C7–C8) was also found to be a chair with the following puckering parameters, Q_T = 0.563 (10) Å, θ = 168.2º (10), φ = 240º(5), which are significantly deviate from the ideal chair parameters than the piperidine ring. Hence, from the complete single crystal XRD analysis, it is confirmed that the molecule exists in a twin-chair conformation with equatorial disposition of both phenyl groups adjacent to the secondary amine group; the two benzene rings are inclined to each other at an angle of 115.86º (calculated value is 115.8º). The bond parameters such as bond length (Å), bond angle (º), dihedral angle (º) and hydrogen bonding interactions were measured. Bond parameters of ABN crystal structure were compared with computed values to understand the geometry of the molecule. The bond length of Csp^2-Nsp^2 is reported [25] as 1.281Å, for a general case. Accordingly, in this molecule, calculated and experimental value of C3-N29 (sp^2) bond lengths are 1.280 Å and 1.299 Å, respectively. The C-N (sp^3) bond length is obtained as 1.468 Å and 1.465 Å from calculated and experimental methods [25]. Similarly, C-C *sp* and sp^2 hybridized bonds are also lie in their characteristic bond length range. Due to the coincidence in geometrical parameters, molecular structure of single crystal and its optimized molecular structure are in good agreement with each other; molecular structures are shown in Fig. 1 (optimized) and Fig. 2 (XRD). The computed and experimental results are shown in Table-2b.

Molecular orbital theory: MO theory calculation was performed using the TD-DFT/B3LYP/6-31G(d,p) level of theory calculation, the results are presented in Table-3, in which the singlet excited states (n states = 6) transitions were obtained (energy level diagrams of each transition are presented in Fig. 3a-f). The first excited state (ES_1) transition lies between HOMO

TABLE-1
CRYSTALLOGRAPHIC DATA AND STRUCTURE REFINEMENT PARAMETERS OF ABN-OBn

Identification code	ABN-OB
Chemical formula	$C_{27}H_{28}N_2O$
M_r	396.51
Crystal system	Tricilinic
Space group	P-1
Temperature (K)	273 (2) K
a, b, c (Å)	a = 8.6884 (7) Å, b = 9.6961 (9) Å, c = 14.1567 (12) Å
α, β, γ (°)	α =73.640(5)°, β = 78.505 (4)°, γ = 87.078 (4)°
V (Å^3)	1121.35 (17) Å^3
Z, Calculated density	2, 1.174 Mg/m^3
Absorption coefficient	0.071 mm^{-1}
F(000)	424
θ range for data collection	1.53 to 28.31°
Limiting indices	-11<=h<=11, -12<=k<=12, -18<=l<=18
Reflections collected/unique	13758/4801 [R(int) = 0.0632]
Completeness to θ = 25.00	96.3 %
Absorption correction	None
Refinement method	Full-matrix least-squares on F^2
Data/restraints/parameters	4801/4/275
Goodness-of-fit on F^2	0.994
Final R indices [I>2σ(I)]	R1 = 0.0758, wR2 = 0.1973
R indices (all data)	R1 = 0.2555, wR2 = 0.2787
Largest diff. peak and hole	0.273 and -0.197 e.A^{-3}

TABLE-2a
PUCKERING PARAMETERS OF PIPERIDINE AND CYCLOHEXANE RINGS OF ABN-OBn CRYSTAL STRUCTURE

Puckering parameters	Q_T	θ	φ
Piperidine ring C1–C2–C3–C4–C5–N1)	0.575 (9) Å	3.9°(9)°	190°
Cyclohexane ring (C2–C3–C4–C6–C7–C8)	0.563 (10) Å	168.2° (10)	240°(5)

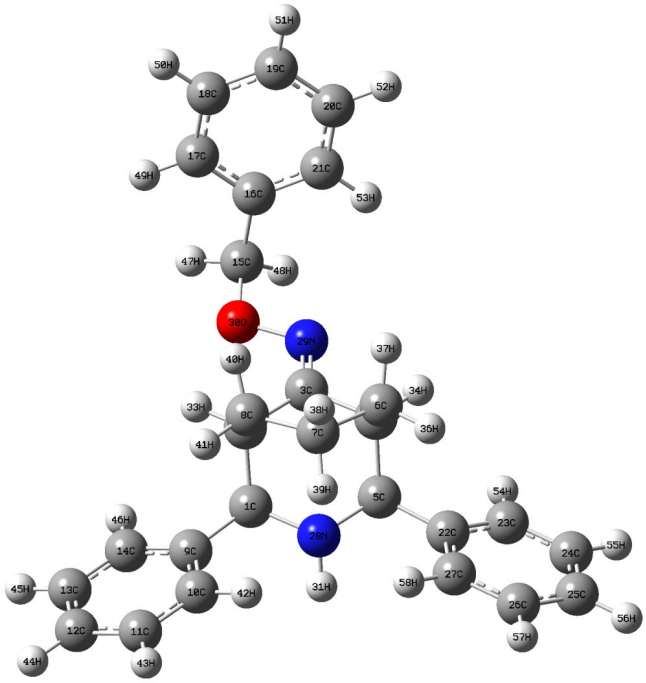

Fig. 1. Optimized molecular structure of ABN-OBn

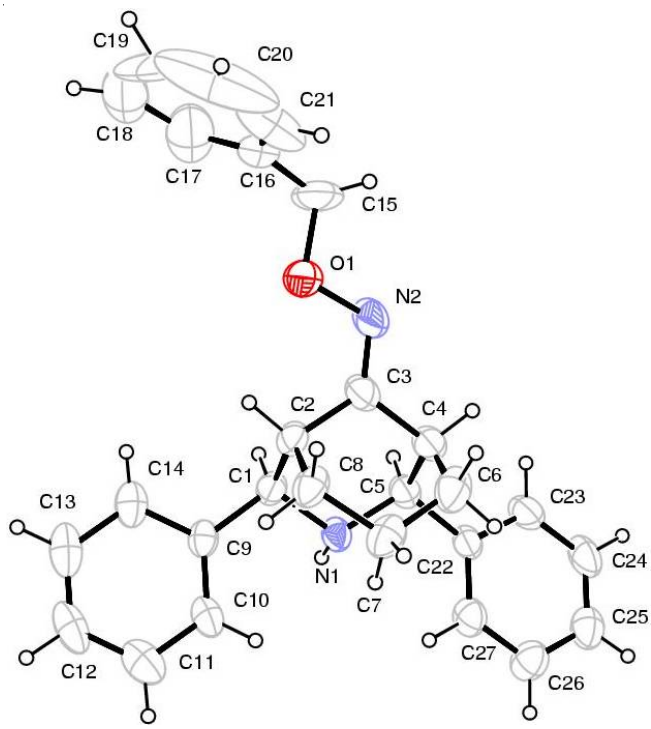

Fig. 2. Crystal structure of ABN-OBn (CCDC No. 1861932)

(H) and LUMO (L), H→L, its excitation energy is 5.0514 eV/246 nm, in second excited state, there were six intermediate transitions occurred as shown in energy level diagram (Fig. 3a-f) its transition energy is calculated about 5.223 eV/237 nm, whereas, the oscillator strength "f" of the transition is 0.0064. Of them, the intense transitions are H→L_{+2} and H→L_{+3} (106→109, 106→110), which is due to $2p_z$ electron excitation in atoms 1-5, 15, 16 and 28-30 of the molecule. In ES_3, there were seven combined electronic transitions as shown in Fig. 3c,

TABLE-2b
BOND PARAMETERS OF BOTH DFT (THEORETICAL) AND XRD (EXPERIMENTAL) STUDIES

Bond	Bond length (Å)		Bond	Angles (°)	
	Theor.	Exp.		Theor.	Exp.
C1-C2	1.566	1.540	C2-C1-C9	112.44	111.6
C1-C9	1.520	1.520	C2-C1-N28	110.27	110.1
C1-N28	1.469	1.465	C9-C1-N28	111.31	111.6
C1-H32	1.107	0.980	C1-C2-C3	106.30	107.4
C2-C3	1.507	1.496	C1-C2-C8	115.92	114.6
C2-C8	1.550	1.543	C3-C2-C8	108.16	108.5
C3-C4	1.506	1.488	C2-C3-C4	112.45	111.9
C3-N29	1.280	1.299	C2-C3-N29	128.84	129.0
C4-C5	1.565	1.550	C4-C3-N29	118.67	119.0
C4-C6	1.549	1.507	C3-C4-C5	106.56	107.2
C5-C22	1.520	1.515	C3-C4-C6	108.61	107.2
C5-N28	1.468	1.465	C5-C4-C6	115.86	115.8
C6-C7	1.541	1.515	C4-C5-C22	112.78	111.6
C7-C8	1.541	1.518	C4-C5-N28	110.01	109.2
C15-C16	1.511	1.503	C22-C5-N28	111.37	111.6
C15-O30	1.436	1.454	C4-C6-C7	113.95	114.9
N29-O30	1.413	1.399	C2-C8-C7	114.26	114.0
			C1-N28-C5	114.50	115.0

TABLE-3
SINGLET EXCITED ELECTRONIC TRANSITIONS OF ABN-OBn CRYSTAL

Singlet excited electronic transitions	Band gap (eV/nm)	Oscillator strength
H→L	5.0514/245.45	0.0747
H_{-1}→L	5.2233/237.00	0.0064
H_{-7}→L, H_{-7}→L_{+1}, H_{-7}→L_{+3}	5.2309/237.02	0.0016
H_{-2}→L, H_{-1}+L	5.2509/236.12	0.0211
H_{-6}→L, H_{-2}→L, H_{-2}→L_{+1}, H→L_{+1}	5.3017/233.86	0.0161
H_{-9}→L, H_{-9}→L_{+1}, H_{-6}→L, H_{-4}→L	5.3846/230.26	0.0012

where the intense transition is H→L_{+3} (106→110). Similarly in ES_4, ES_5 and ES_6, the intense transition is due to atoms involved in HOMO (106) level and L_{+2}(109), L_{+4}(111) and L_{+5}(112) levels, respectively. All the transition in ES_3, $2p_z$, 3s and $3p_z$ electrons are majorly involved, especially the nitrogen (N_{29}) acquires more negative coefficient (-0.1714 -$2p_z$,) than the other atoms.

Frontier molecular orbital calculation was performed using B3LYP/6-31G(d,p) level of theory calculation. The HOMO mainly localizes on the azabicycle and LUMO locate on the phenyl rings. The band gap between HOMO and LUMO is -5.742 eV.

NBO analysis: The NBO analysis performed using B3LYP/6-31G(d,p) level of theory calculation. The natural atomic orbital (NAO) and natural bond orbital (NBO) analysis were performed using Gaussian NBO version 3.1. The obtained results are presented in Table-4. The core level atomic orbital population was calculated as 59.97e and valence orbital population was calculated as 151.50e, whereas, the total minimal basis is 211.47e and Rydberg basis (Non-Lewis) was accounted as 0.523e. The NBO analysis shows that the core electrons as 59.97e, valence Lewis electrons as 147.32e and total Lewis electrons as 207.30e.

Donor and acceptor bonds, electron densities and hyper-conjugative (E^2) interaction energies are given in Table-4. In NBO investigation, we mainly concentrate on the π-π* inter-

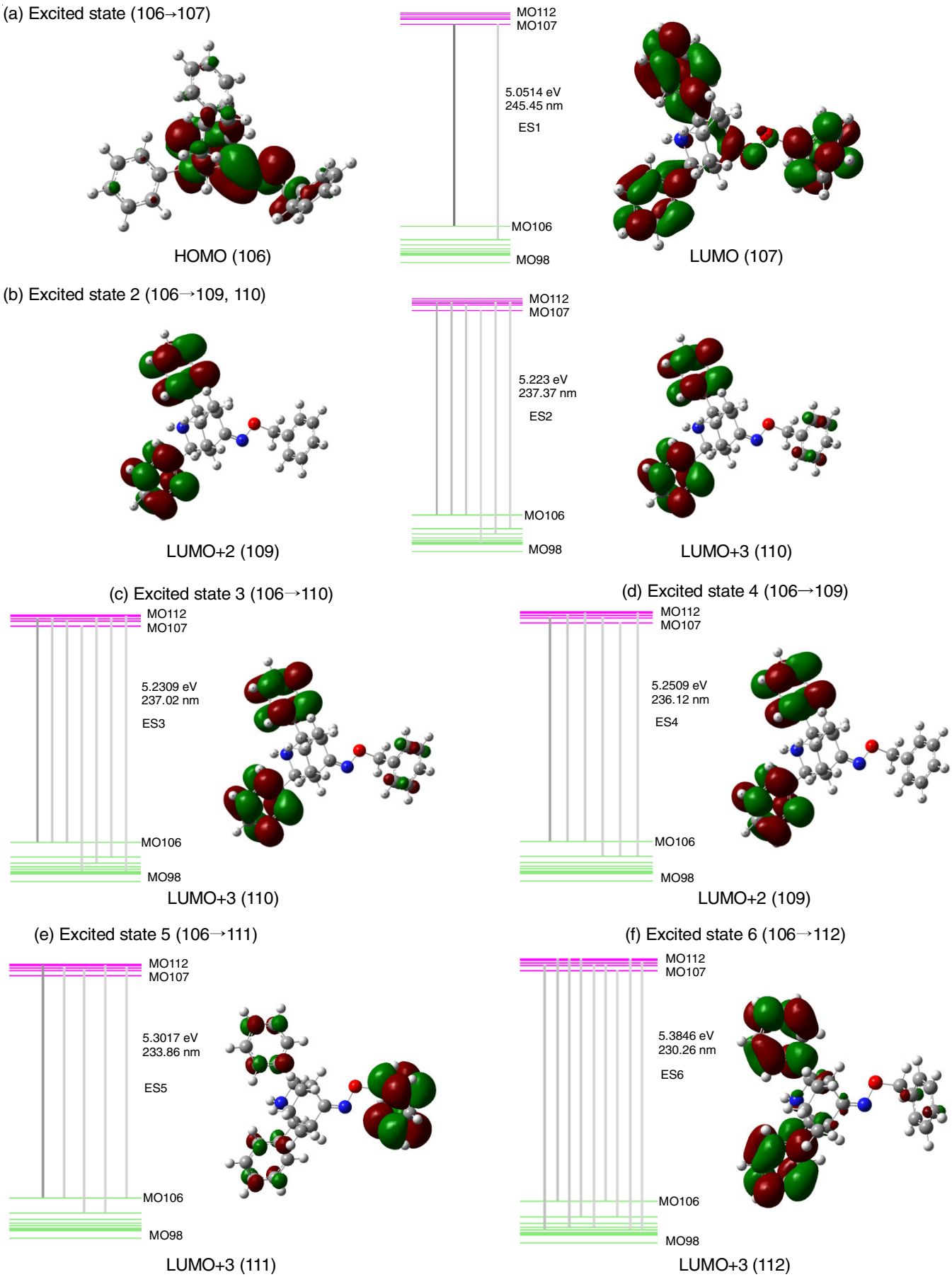

Fig. 3. Electronic transitions along with frontier molecular orbitals of ABN-OBn

TABLE-4
SECOND ORDER PERTURBATION THEORY ANALYSIS OF NBO BASIS FOR ABN-OBn

Bond type	Donor (i)	ED	Acceptor (j)	ED	[a]$E^{(2)}$ kJ/mol	[b]E(j)-E(i)	[c]F(i,j)
σ-σ*	C1-N28	1.98402	C1-C9	0.02989	2.09	1.13	0.021
			C5-C22	0.02980	3.97	1.19	0.030
			C5-N28	0.02170	2.76	1.06	0.024
			C9-C14	0.02120	7.11	1.28	0.042
σ-σ*	C3-N29	1.9889	C2-C3	0.04434	9.58	1.33	0.050
			C3-C4	0.03027	6.99	1.33	0.042
			C15-O30	0.03057	7.66	1.20	0.042
σ-σ*	C3-N29	1.97213	C1-C2	0.03879	7.82	0.67	0.032
			C2-C8	0.02293	7.70	0.70	0.032
			C4-C5	0.04039	9.46	0.67	0.035
			C4-C6	0.02449	9.62	0.70	0.036
π-π*	C9 - C10	1.65457	C11-C12	0.33039	87.53	0.28	0.069
			C13-C14	0.32586	82.72	0.28	0.067
π-π*	C11-C12	1.66720	C9-C10	0.34427	82.51	0.28	0.067
			C13-C14	0.32586	85.98	0.28	0.068
π-π*	C13-C14	1.67346	C9-C10	0.34427	86.15	0.29	0.069
			C11-C12	0.33039	82.84	0.28	0.067
π-π*	C16-C21	1.64483	C17-C18	0.32681	86.86	0.28	0.068
			C19-C20	0.33368	86.27	0.28	0.068
π-π*	C17-C18	1.66661	C16-C21	0.34458	84.06	0.29	0.068
			C19-C20	0.33368	85.77	0.28	0.068
π-π*	C19- C20	1.66261	C16-C21	0.34458	84.73	0.29	0.068
			C17-C18	0.32681	83.93	0.28	0.067
π-π*	C22-C27	1.65459	C23-C24	0.32612	82.76	0.28	0.067
			C25-C26	0.33021	87.53	0.28	0.069
π-π*	C23-C24	1.67384	C22-C27	0.34400	86.11	0.29	0.069
			C25-C26	0.33021	82.72	0.28	0.067
π-π*	C25-C26	1.66714	C22-C27	0.34400	82.47	0.28	0.067
			C23-C24	0.32612	86.11	0.28	0.068
σ-σ*	N29-O30	1.98186	C3-C4	0.03027	21.58	1.19	0.070
n-σ*	nO30	1.88699	C3-N29	0.13601	66.44	0.34	0.066

[a]$E^{(2)}$ means energy of hyper conjugative interaction (stabilization energy); [b]Energy difference between donor 'i' and acceptor 'j' NBO orbitals; [c]F(i,j) is the fork matrix element between 'i' and 'j' NBO orbitals.

actions, where, π is a donor and π* is an acceptor. This investigation indicates that the contribution of nitrogen atoms is less, especially, delocalization of energy during the interaction of nitrogen bonds (σC1-N28, σC3-N29 and πC3-N29) is shown to be minimum in this molecule, whereas, carbon-carbon bond interactions obtained more E^2 energy. For instance, charge delocalization between C9-C10 and C11-C12 has 87.53 kJ/mol of energy. Similarly, the average energy of C-C interactions is 82 kJ/mol for the whole molecule. On the other hand, oxygen atom has appreciable E^2 energy during σN29-O30→σ*C3-C4 and nO30'→π*C3-N29 interactions and they are 21.58 and 66.44kJ/mol, respectively.

Density of states (DOS): Using Multiwfn 3.4.1 version [26], density of states of ABN-OBn was studied. Density of states is an important concept of solid state physics, which represents the number of states in unit energy interval. In an isolated system, the energy levels are discrete, though the concept of DOS is insignificant in single isolated organic molecule, if the discrete energy levels are broadened to curve artificially, the DOS graph can be used as a valuable tool for analyzing the nature of electron density.

The original total density of states (TDOS) of isolated system can be written as:

$$TDOS(E) = \sum_i \delta(E - \varepsilon_i) \quad (1)$$

where ε is Eigen value set of single-particle Hamilton, δ is Dirac delta function. If δ is replaced by broadening function F(x), such as Gaussian, Lorentzian and pseudo-Voigt function, we get broadened TDOS [26].

In ABN-OBn, the molecular orbitals (MOs) are fragmented and plotted the electron density of each fragments as shown in Fig. 4. The vertical dashed line indicates Fermi energy level. The original DOS graph has discrete comb-like lines and in fact, it is difficult to distinguish the discrete lines. While broadening the discrete lines (the black curve is TDOS) it is convenient to realize the dense of energy levels distributed. Besides, the PDOS is separated as fragments f1-f4, the f1 (red curve) belongs to C1-C8 group, which has a considerable contribution in the HOMO level and the f2 (blue line) belongs to N28 and N29, shows a meager contribution, whereas, the f3 (pink line) with maximum contribution due to the presence of oxygen in the molecule. Similar to f1, the fragment f4 (C9-C27/gray) also contributes a considerable electron density. In addition, the fragments f1 and f4 contribute to the unoccupied levels as well. On the whole, the OPDOS magnitude is much smaller than TDOS and PDOS.

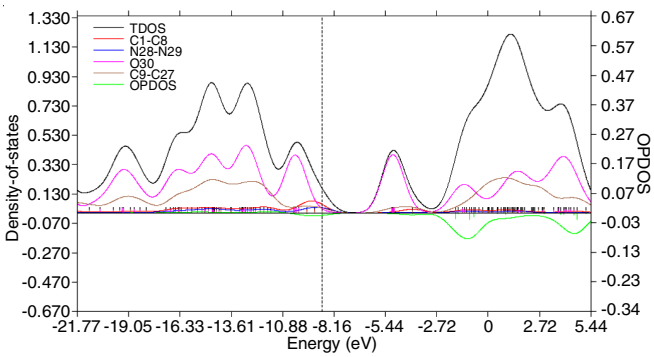

Fig. 4. Density of states (DOS) with respect to functional groups in ABN-OBn molecule

Non-linear property analysis: Theoretical investigation plays a substantial role in understanding the quantitative structure property relationship (QSPR), which is able to assist in designing novel NLO materials. A molecule to be NLO active, it is important to have high hyperpolarizability (β_0) values. The calculated values of β_0 by finite field approach method are given in Table-5 along with the corresponding components.

TABLE-5
HYPERPOLARIZABILITY (β_0), POLARIZABILITY (α) AND DIPOLE MOMENT (μ) OF ABN-OBn

Parameters	Values	Parameters	Values
β_{xxx}	-129.87	α_{xx}	331.3206
β_{xxy}	-15.90	α_{xy}	14.1323
β_{xyy}	17.72	α_{yy}	322.4904
β_{yyy}	19.29	α_{xz}	17.3651
β_{xxz}	-14.92	α_{yz}	-10.7406
β_{xyz}	-51.82	α_{zz}	217.77
β_{yyz}	-24.03	α	0.726×10^{-33}
β_{xzz}	56.04	μ_x	-0.205
β_{yzz}	-50.31	μ_y	0.189
β_{zzz}	70.47	μ_z	-0.139
β	0.6881×10^{-30} esu	μ	0.3113 Debye

*Urea (standard) = 0.3728×10^{-30} esu

For ABN-OBn, we have obtained high value of β_{xxx}, β_{xxy} and β_{xyy} components (Table-5) thus indicating that there is a charge imbalance along the *y*-axis due to the high electronegative oxygen atom lying in the X–Y plane. The β_0 value (0.6881×10^{-30} esu) also indicates that the compound has very lower nonlinear optical property. This compound has lower β_0 coefficient but higher than that of urea. Urea is one of the prototype molecules used in the study of the NLO properties of molecular systems. Therefore, it is used frequently as a threshold value for comparative purposes [27].

Hirshfeld surface analysis: Hirshfeld surface (HSs) and 2D fingerprint plot as shown in Fig. 5a-j were generated using Crystal Explorer 3.1, based on the results of single crystal X-ray diffraction. The crystal packing builds through the N···H-C interactions, where the crystal units are in zigzag pattern by means of anti-parallel packing of molecules. The function of d_{norm} is a ratio encompassing the distances of any surface point to the nearest interior (d_i) atom, exterior (d_e) atom and the van der Waals radii of the atoms [28]. The negative value of d_{norm} indicates the sum of d_i and d_e, which is shorter than the sum of the relevant van der Waals radii. It is considered to be in the closest contact and visualized as red in the Hirshfeld surface. The white colour denotes intermolecular distances closer to van der Waals contacts with d_{norm} equal to zero, whereas contacts longer than the sum of van der Waals radii with positive d_{norm} values are coloured as blue. A plot of d_i *versus* d_e is 2D fingerprint plots that recognize the existence of different types of intermolecular interactions. In the shape index, the highlighted red and blue triangles shown by purple ellipse indicate that the π···π interactions identically present in the crystal structure and its 2D fingerprint shows the 72% contribution by C···C contact of the Hirshfeld surface. Red and blue triangles patterns show explicitly how the molecule overlaps and contact with one another. Red triangle represents the carbon atoms present in the benzene ring of molecule outside the surface, while blue represents the carbon atoms of benzene ring inside the molecule. The curvedness surface indicates the electron density surface curves around the molecular interactions [29]. Moreover, the flat green region separated by the blue edges in curvedness surface is another characteristic of π···π stacking. The deep red spots in the d_e surface are responsible for strong interactions of C-H (6.2%), C-N (6.3%) and C-O (3.8%).

Conclusion

The target ABN-OBn single crystal belongs to triclinic system with P-1 space group. From the XRD analysis, it is clear that the molecule exists in a twin-chair conformation with equatorial disposition of the substituents. The two benzene rings on both sides of the secondary amine group of the azabicycle are inclined to each other at an angle of 115.86º. From the puckering data [$Q_T = 0.575(9)$ Å and $\theta = 3.9$º], it is concluded that the piperidone ring of the azabicycle is comparatively closer to the ideal chair conformation, whereas, the cyclohexane deviates significantly as witnessed by its Q_T (0.563) Å and θ (168.2º). According to computational data, among the electronic transitions ES_1 to ES_6 (n = 6 states), ES_3 transition plays a major role, where, the electron occupancies predominantly lie in $2p_z$, $3s$ and $3p_z$ orbitals owing to the presence of nitrogen (N_{29}), which has a higher negative coefficient (-0.1714e) than the other atoms in the molecule. FMO analysis reveals that the highest occupied molecular orbital mainly localized on the azabicycle, whereas, the lowest unoccupied molecular orbital locates on the phenyl rings; the band gap was found to be -5.742 eV. NBO interaction shows that the C-C bond obtained more E^2 energy, whereas, the average energy of C-C inter-actions is 82 kJ/mol for the whole molecule. In DOS analysis, fragment f1 (red curve) belongs to C1-C6 group has a consi-derable contribution in the HOMO level. This molecule has no significant β_0 value, which indicates that the compound has very lower optical behaviour. ABN-OBn crystal 2D fingerprint shows that the C···C contact contributes 72% Hirshfeld surface. On the whole, this molecule mainly driven by carbon-carbon bonding and does not exhibit significant optical or electronic properties but the architecture of molecular structure is interesting with informative geometrical parameters.

Appendix A: Data collection [30-32]**:** APEX2 [30]; cell refinement: SAINT Bruker [30]; data reduction: SAINT Bruker

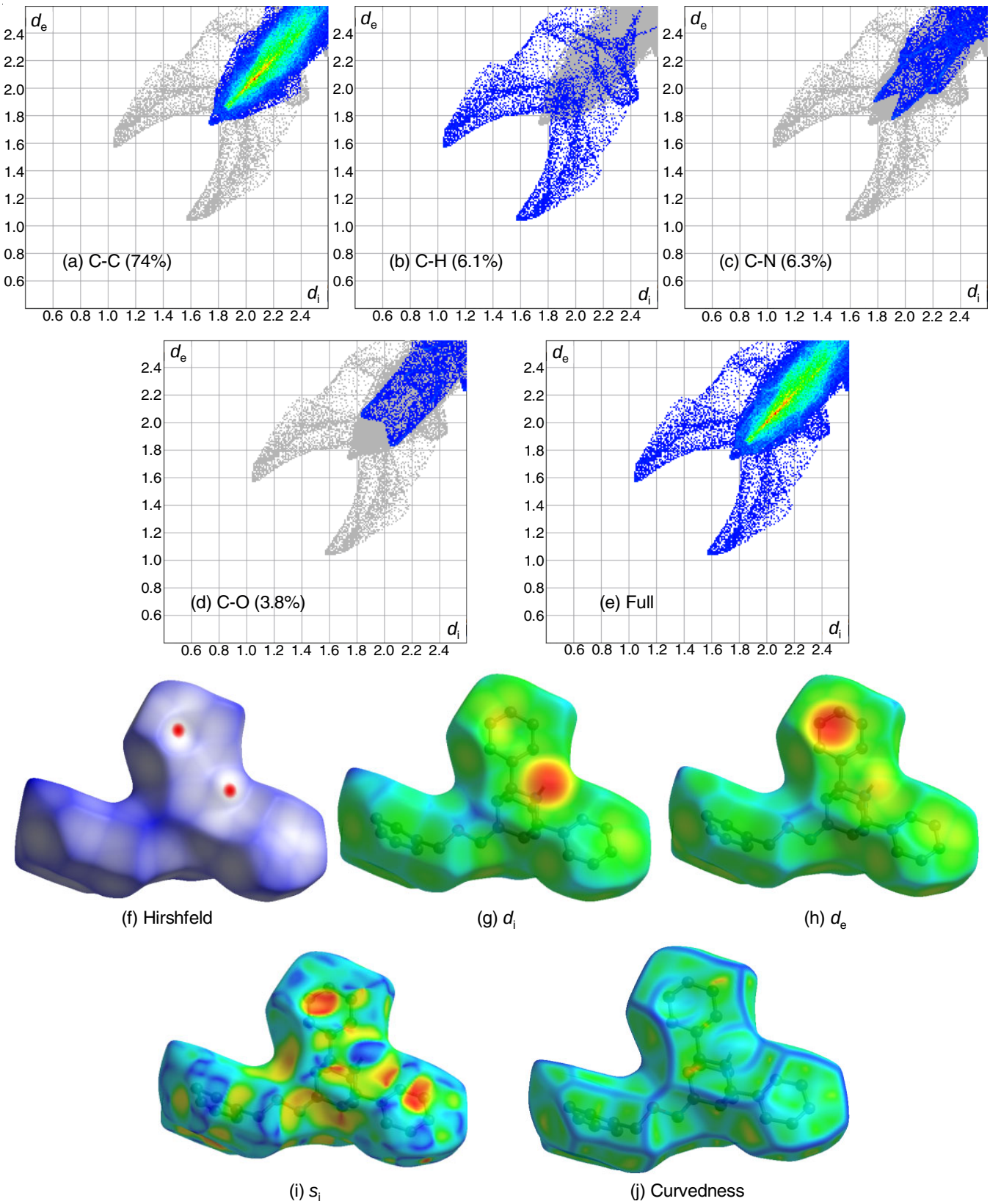

Fig. 5. Hirshfeld surface analysis of ABN-OBn

[30]; program(s) used to solve structure: SHELXS97 [31]; program(s) used to refine structure: SHELXL97 [31]; molecular graphics: ORTEP-3 [32]; software used to prepare material for publication: SHELXL97 [31].

CONFLICT OF INTEREST

The authors declare that there is no conflict of interests regarding the publication of this article.

REFERENCES

1. R. Jeyaraman and S. Avila, *Chem. Rev*., **81**, 149 (1981); https://doi.org/10.1021/cr00042a002
2. D. Paterson and A. Nordberg, *Prog. Neurobiol.*, **61**, 75 (2000); https://doi.org/10.1016/S0301-0082(99)00045-3
3. M. Ganesan, N. Chandrasekaran and K. Ramarajan, *Indian J. Chem.*, **40B**, 96 (2001).
4. D.L. Bryant, R.B. Free, S.M. Thomasy, D.J. Lapinsky, K.A. Ismail, S.B. McKay, S.C. Bergmeier and D.B. McKay, *Neurosci. Res.*, **42**, 57 (2002); https://doi.org/10.1016/S0168-0102(01)00304-2
5. K.A. Ismail and S.C. Bergmeier, *Eur. J. Med. Chem.*, **37**, 469 (2002); https://doi.org/10.1016/S0223-5234(02)01353-3
6. D.J. Hardick, I.S. Blagbrough, G. Cooper, B.V.L. Potter, T. Critchley and S. Wonnacott, *J. Med. Chem.*, **39**, 4860 (1996); https://doi.org/10.1021/jm9604991
7. D. Barker, D.H.-S. Lin, J.E. Carland, C.P.-Y. Chu, M. Chebib, M.A. Brimble, G.P. Savage and M.D. McLeod, *Bioorg. Med. Chem.*, **13**, 4565 (2005); https://doi.org/10.1016/j.bmc.2005.04.054
8. K.J. Goodall, M.A. Brimble and D. Barker, *Magn. Reson. Chem.*, **44**, 980 (2006); https://doi.org/10.1002/mrc.1878
9. M.S. Arias, Y.G. Smeyers, M.S. Fernandez, N.J. Smeyers, E. Galvez, I. Fonseca and J.S. Aparicio, *J. Org. Chem.*, **59**, 2565 (1994); https://doi.org/10.1021/jo00088a044
10. M.S. Arias-Perez, A. Alejo and A. Maroto, *Tetrahedron*, **53**, 13099 (1997); https://doi.org/10.1016/S0040-4020(97)00832-6
11. T. Poloñski, M. Pham, M.J. Milewska and M. Gdaniec, *J. Org. Chem.*, **61**, 3766 (1996); https://doi.org/10.1021/jo9600159
12. D.H. Park, J. Venkatesan, S.K. Kim, V. Ramkumar and P. Parthiban, *Bioorg. Med. Chem. Lett.*, **22**, 6362 (2012); https://doi.org/10.1016/j.bmcl.2012.08.080
13. D.H. Park, J. Venkatesan, S.-K. Kim and P. Parthiban, *Bioorg. Med. Chem. Lett.*, **22**, 6004 (2012); https://doi.org/10.1016/j.bmcl.2012.06.071
14. D.H. Park, Y.T. Jeong and P. Parthiban, *J. Mol. Struct.*, **1005**, 31 (2011); https://doi.org/10.1016/j.molstruc.2011.08.006
15. P. Parthiban, G. Aridoss, P. Rathika, V. Ramkumar and S. Kabilan, *Bioorg. Med. Chem. Lett.*, **19**, 6981 (2009); https://doi.org/10.1016/j.bmcl.2009.10.042
16. O. Mazimba and K. Mosarwa, *Int. J. Chem. Stud.*, **2**, 22 (2015).
17. A. Kamaraj, R. Rajkumar and K. Krishnasamy, *J. Mol. Struct.*, **1088**, 179 (2015); https://doi.org/10.1016/j.molstruc.2015.01.044
18. P. Parthiban, S. Balasubramanian, G. Aridoss and S. Kabilan, *Spectrochim. Acta A Mol. Biomol. Spectrosc.*, **70A**, 11 (2008); https://doi.org/10.1016/j.saa.2007.07.059
19. P. Parthiban, M. Rani and S. Kabilan, *Monatsh. Chem.*, **140**, 287 (2009); https://doi.org/10.1007/s00706-008-0021-6
20. P. Parthiban, R. Ramachandran, G. Aridoss and S. Kabilan, *Magn. Reson. Chem.*, **46**, 780 (2008); https://doi.org/10.1002/mrc.2243
21. P. Parthiban, P. Rathika, V. Ramkumar, S.M. Son and Y.T. Jeong, *Bioorg. Med. Chem. Lett.*, **20**, 1642 (2010); https://doi.org/10.1016/j.bmcl.2010.01.048
22. M.J. Frisch, G.W. Trucks, H.B. Schlegel, G.E. Scuseria, M.A. Robb, J.R. Cheeseman, J.A. Montgomery Jr., T. Vreven, K.N. Kudin, J.C. Burant, J.M. Millam, S.S. Iyengar, J. Tomasi, V. Barone, B. Mennucci, M. Cossi, G. Scalmani, N. Rega, G.A. Petersson, H. Nakatsuji, M. Hada, M. Ehara, K. Toyota, R. Fukuda, J. Hasegawa, M. Ishida, T. Nakajima, Y. Honda, O. Kitao, H. Nakai, M. Klene, X. Li, J.E. Knox, H.P. Hratchian, J.B. Cross, O. Yazyev, V. Bakken, C. Adamo, J. Jaramillo, R. Gomperts, R.E. Stratmann, A.J. Austin, R. Cammi, C. Pomelli, J.W. Ochterski, P.Y. Ayala, K. Morokuma, G.A. Voth, P. Salvador, J.J. Dannenberg, V.G. Zakrzewski, S. Dapprich, A.D. Daniels, M.C. Strain, O. Farkas, D.K. Malick, A.D. Rabuck, K. Raghavachari, J.B. Foresman, J.V. Ortiz, Q. Cui, A.G. Baboul, S. Clifford, J. Cioslowski, B.B. Stefanov, G. Liu, A. Liashenko, P. Piskorz, I. Komaromi, R.L. Martin, D.J. Fox, T. Keith, M.A. Al-Laham, C.Y. Peng, A. Nanayakkara, M. Challacombe, P.M.W. Gill, B. Johnson, W. Chen, M.W. Wong, C. Gonzalez and J.A. Pople, Gaussian 03, Revision C.02, Gaussian Inc., Wallingford, CT (2004).
23. S.K. Wolff, D.J. Grimwood, J.J. McKinnon, M.J. Turner, D. Jayatilaka and M.A. Spackman, Crystal Explorer 17 (2017).
24. D. Cremer and J.A. Pople, *J. Am. Chem. Soc.*, **97**, 1354 (1975); https://doi.org/10.1021/ja00839a011
25. F.H. Allen, O. Kennard, D.G. Watson, L. Brammer, A.G. Orpen and R. Taylor, *J. Chem. Soc. Perkin Trans. II*, S1 (1987); https://doi.org/10.1039/p298700000s1
26. T. Lu and F. Chen, *J. Comput. Chem.*, **33**, 580 (2012); https://doi.org/10.1002/jcc.22885
27. M. Özdemir, M. Sönmez, F. Sen, M. Dinçer and N. Özdemir, *Spectrochim. Acta A Mol. Biomol. Spectrosc.*, **137**, 1304 (2015); https://doi.org/10.1016/j.saa.2014.08.131
28. J. Dalal, N. Sinha, H. Yadav and B. Kumar, *RSC Adv.*, **5**, 57735 (2015); https://doi.org/10.1039/C5RA10501C
29. V. Meenatchi, R. Agilandeshwari and S.P. Meenakshisundaram, *RSC Adv.*, **5**, 71076 (2015); https://doi.org/10.1039/C5RA07936E
30. Bruker, APEX2, SAINT and SADABS, Bruker AXS Inc., Madison, Wisconsin, USA (2004).
31. G.M. Sheldrick, *Acta Crystallogr. A*, **64**, 112 (2008); https://doi.org/10.1107/S0108767307043930
32. L.J. Farrugia, *J. Appl. Cryst.*, **30**, 565 (1997); https://doi.org/10.1107/S0021889897003117